



# A high-resolution laser ablation study of the $\tilde{A}^2\Pi-\tilde{X}^2\Sigma^+$ transition of SrCCH

M.J. Dick<sup>a</sup>, P.M. Sheridan<sup>b</sup>, J.-G. Wang<sup>b</sup>, P.F. Bernath<sup>a,b,\*</sup>

<sup>a</sup> Department of Physics, University of Waterloo, Waterloo, Ont., Canada N2L 3G1

<sup>b</sup> Department of Chemistry, University of Waterloo, Waterloo, Ont., Canada N2L 3G1

Received 5 May 2005; in revised form 14 June 2005

## Abstract

The laser-induced excitation spectrum of the  $\tilde{A}^2\Pi-\tilde{X}^2\Sigma^+$  transition of SrCCH has been recorded at high resolution. A rotational analysis has been performed yielding rotational and fine structure parameters for the  $\tilde{A}$  state. In addition, a vibrational frequency for the Sr–C stretch ( $\nu_3$ ) in the  $\tilde{A}^2\Pi$  state has been determined. Using the rotational constant of the  $\tilde{A}$  state, the Sr–C bond length was determined to be 2.43 Å, which is  $\sim 0.03$  Å shorter than in the ground state. A comparison of the  $\Lambda$ -doubling constant  $p$ , to those of the other alkaline-earth acetylides suggests that SrCCH and CaCCH appear to follow the pure precession model unlike MgCCH. Finally, a search for the  $\tilde{B}^2\Sigma^+-\tilde{X}^2\Sigma^+$  transition was negative, as with CaCCH, suggesting that the  $\tilde{B}$  state may be predissociative. © 2005 Elsevier Inc. All rights reserved.

**Keywords:** SrCCH; Strontium-bearing molecules; Monoacetylides; Laser spectroscopy; Alkaline-earth metal bond

## 1. Introduction

Unlike their diatomic counterparts, metal containing polyatomic molecules have been the focus of a limited number of gas phase spectroscopic studies. However, for one such class of molecule, the metal monoacetylides, work has progressed steadily over the past 20 years. These investigations, which include both theory and experiment, have focused mainly on the alkali and alkaline-earth metals with only a few notable exceptions, Cr and Yb [1,2], having been completed. A brief summary of this work follows.

Experimentally, the alkali metal monoacetylides have been studied in their ground states by millimeter wave spectroscopy. From the pure rotational spectra of LiCCH, NaCCH, and KCCH [3–6], each species has been shown to be linear in its  $^1\Sigma^+$  ground state.

This work is in agreement with Scalmani et al. [7] who have investigated the electronic properties of these molecules using ab initio methods. Unfortunately, no information is available for the excited electronic states of these species perhaps because these excited states are not bound.

The alkaline-earth monoacetylides have been the subject of more extensive investigations than their alkali counterparts. The ground electronic states of MgCCH, CaCCH, and SrCCH ( $^2\Sigma^+$ ) have been studied by several experimental techniques [5,8–11] as well as by ab initio calculations [12–14]. In addition, experimental data exist for the excited states of these molecules. For CaCCH, the  $\tilde{A}^2\Pi-\tilde{X}^2\Sigma^+$  transition has been observed experimentally both at low [15,16] and high resolution [17–21], including a determination of the dipole moments for the  $\tilde{A}$  and  $\tilde{X}$  states of CaCCH using Stark spectroscopy [22]. In addition, the  $\tilde{C}^2\Delta-\tilde{X}^2\Sigma^+$  transition [23] of CaCCH has been observed at low resolution. The  $\tilde{A}^2\Pi-\tilde{X}^2\Sigma^+$  transition of MgCCH has also been examined both at

\* Corresponding author. Fax: +1 519 746 0435.

E-mail address: bernath@uwaterloo.ca (P.F. Bernath).

low [24,25] and recently at high resolution [26]. The  $\tilde{A}-\tilde{X}$  transition of SrCCH was first observed by Bernath and co-workers [15] at low resolution, while Ellis and co-worker [27] have reported measurements of the  $\tilde{B}^2\Delta-\tilde{X}^2\Sigma^+$  transition at low resolution.

In this work, we report the first high-resolution spectroscopic analysis of the  $\tilde{A}^2\Pi-\tilde{X}^2\Sigma^+$  transition of SrCCH. For the  $\tilde{A}^2\Pi$  state rotational and fine structure constants have been determined. Trends in the geometries and  $\Lambda$ -doubling constants for the alkaline-earth monoacetylides will be discussed.

## 2. Experimental

The  $\tilde{A}-\tilde{X}$  transition of SrCCH was observed using the laser ablation source of the Bernath group at the University of Waterloo. This instrument has been described in detail previously [28] and, therefore, only minor modifications made for this study will be discussed. In our work, the third harmonic (355 nm) of a pulsed (10 Hz) Nd/YAG laser (10 mJ/pulse) was used to vaporize a strontium target rod. (The first and second harmonics were found to produce a weaker SrCCH signal). The molecular jet was formed by the expansion of a 7% gas mixture of HCCH in Ar at a backing pressure of 100 psi, resulting in a rotational temperature of only 4–6 K. Following the recent work on MgCCH [26] a 10% mixture of CH<sub>4</sub> in Ar was tested as the reactant gas mixture, but HCCH was found to yield stronger SrCCH signals. Finally, the molecular expansion was not skimmed; instead the probe laser interrogated a free jet expansion  $\sim 15$  cm downstream. As before, band pass filters ( $\pm 20$  nm) were used to attenuate most of the plasma radiation from the ablation source.

Low-resolution spectra were obtained using an Ar<sup>+</sup>-pumped linear dye laser operating with DCM laser dye. This laser has a linewidth of 30 GHz and a maximum power of 800 mW when the pump power is 5 W. A typical scan rate of  $\sim 1000$  cm<sup>-1</sup> in 20 min was employed. Signals from the boxcar integrator and frequency readings from a wavemeter (Burleigh WA-2500 Wavemeter Jr) were processed using a data acquisition program written in Labview.

High-resolution spectra were obtained using a Coherent Autoscan 699-29 ring dye laser system. This laser has a linewidth of 10 MHz. The spectra were calibrated using I<sub>2</sub> lines, [29] which were recorded at the same time as the experimental data. A typical spectrum was taken in 5 cm<sup>-1</sup> segments at a scan speed of 60 s per wavenumber with a data sampling rate of 10 MHz. Several of these scans (4–6) were then averaged together to further increase the signal-to-noise ratio. Typical experimental linewidths were 350 MHz as a result of residual Doppler broadening of the molecular jet as it passes through the detection region.

## 3. Results and analysis

Initially, a broadband survey spectrum was measured for SrCCH over the range 14000–16000 cm<sup>-1</sup>. A portion of this spectrum is shown in Fig. 1. The spin-orbit components of the  $\tilde{A}-\tilde{X}$  ( $0_0^0$ ) transition of SrCCH are clearly visible on the red side of the spectrum. The location of these features at 14182 cm<sup>-1</sup> ( $^2\Pi_{1/2}-^2\Sigma^+$ ) and 14454 cm<sup>-1</sup> ( $^2\Pi_{3/2}-^2\Sigma^+$ ) is consistent with previous observations [15]. Also visible is the  $\tilde{A}^2\Pi-\tilde{X}^2\Sigma^+$  ( $0_0^0$ ) transition of SrOH, which is present as a result of impurities, and the  $^3P_1-^1S_0$  atomic transition of Sr. Two additional small features can be attributed to the ( $\nu_3$ ) Sr–C stretch of SrCCH; the  $^2\Pi_{1/2}-^2\Sigma^+$  ( $3_0^1$ ) transition is located at 14527 cm<sup>-1</sup> and the  $^2\Pi_{3/2}-^2\Sigma^+$  ( $3_0^1$ ) transition is found at 14800 cm<sup>-1</sup>. Unfortunately, the  $^2\Pi_{3/2}-^2\Sigma^+$  ( $3_0^1$ ) transition is overlapped with the  $\tilde{A}^2\Pi_{3/2}-\tilde{X}^2\Sigma^+$  ( $0_0^0$ ) transition of SrOH.

Using the frequency positions determined from the low-resolution study, high-resolution spectra of the  $^2\Pi_{1/2}-^2\Sigma^+$  and  $^2\Pi_{3/2}-^2\Sigma^+$  ( $0_0^0$ ) bands of SrCCH were obtained. In Fig. 2, spectra of these two spin-orbit components are shown, one above the other for comparison. These spectra exhibit a typical Hund's case (a)  $^2\Pi$ —Hund's case (b)  $^2\Sigma^+$  structure for a linear molecule with  $\sim 1B$  and  $\sim 3B$  spaced branches present. The structure of the  $^2\Pi_{1/2}-^2\Sigma^+$  and  $^2\Pi_{3/2}-^2\Sigma^+$  spin components differ as expected, with the  $^2\Pi_{3/2}-^2\Sigma^+$  transition exhibiting a larger origin gap, as well as the  $\sim 1B$  spaced branches of the  $^2\Pi_{1/2}-^2\Sigma^+$  band being more compressed.

High-resolution spectra were also obtained for the ( $3_0^1$ ) bands of the  $^2\Pi_{1/2}-^2\Sigma^+$  and  $^2\Pi_{3/2}-^2\Sigma^+$  transitions.

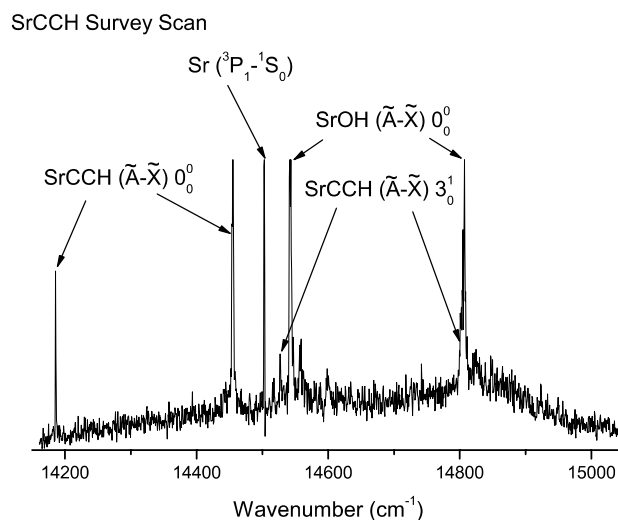


Fig. 1. A section of the low-resolution survey scan over the range  $\sim 14000$ – $15000$  cm<sup>-1</sup>. The spin-orbit components of the  $\tilde{A}^2\Pi-\tilde{X}^2\Sigma^+$  transition of SrCCH are located at 14182 and 14454 cm<sup>-1</sup>. In addition the  $^3P_1-^1S_0$  atomic transition of the Sr atom and the  $\tilde{A}^2\Pi-\tilde{X}^2\Sigma^+$  transition of SrOH (a result of impurities) are present in this spectrum. Also present are the  $\tilde{A}-\tilde{X}$  ( $3_0^1$ ) bands as weak features. The uneven baseline is a result of varying laser power.

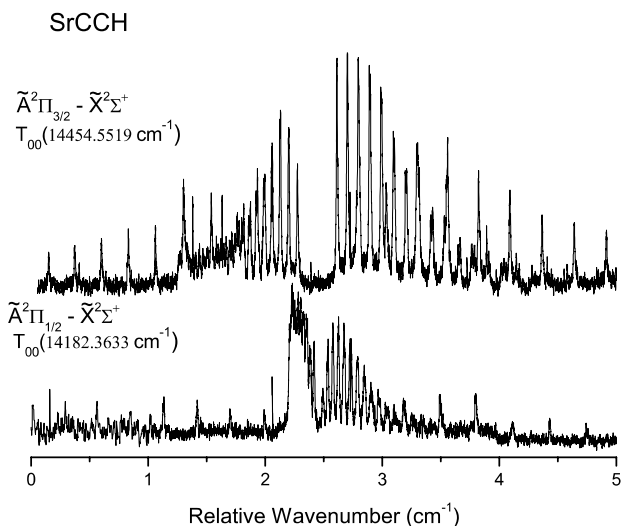


Fig. 2. High-resolution spectra of the two spin-orbit components of the  $\tilde{A}-\tilde{X}$  transition of SrCCH are shown here. The  ${}^2\Pi_{1/2}-{}^2\Sigma^+$  spin component is located in the bottom panel, while the  ${}^2\Pi_{3/2}-{}^2\Sigma^+$  band is displayed above for comparison. The  $\sim 1\text{B}$  and  $\sim 3\text{B}$  spaced lines and the greater origin gap in the  ${}^2\Pi_{3/2}-{}^2\Sigma^+$  band are typical of a Hund's case (a)  ${}^2\Pi$ —Hund's case (b)  ${}^2\Sigma^+$  transition. The greater signal-to-noise ratio in the  ${}^2\Pi_{3/2}-{}^2\Sigma^+$  spectrum is due to better laser power.

Fig. 3 shows a high-resolution spectrum of the  ${}^2\Pi_{1/2}-{}^2\Sigma^+$  ( $3_0^1$ ) band in the top panel, with the corresponding ( $0_0^0$ ) band below for comparison. Unfortunately, the signal-to-noise ratio has significantly decreased in comparison to that of the ( $0_0^0$ ) band, however, a similar structure is still visible between the two. Even at high resolution, the  ${}^2\Pi_{3/2}-{}^2\Sigma^+$  ( $3_0^1$ ) transition proved to be too heavily overlapped with the SrOH  $\tilde{A}^2\Pi_{3/2}-\tilde{X}^2\Sigma^+$  ( $0_0^0$ ) band to obtain a clear spectrum.

Identification of the general branch structure for the  $\tilde{A}^2\Pi-\tilde{X}^2\Sigma^+$  transition of SrCCH was accomplished using

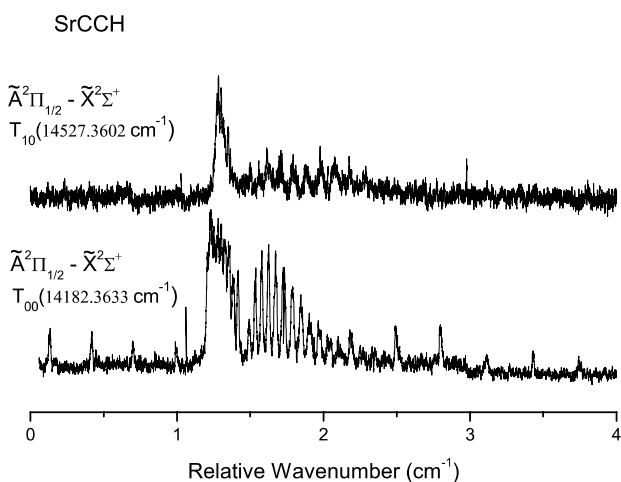


Fig. 3. High-resolution spectra of the lower spin-orbit component of SrCCH in the ( $0_0^0$ ) and ( $3_0^1$  Sr-C stretch) bands of the  $\tilde{A}-\tilde{X}$  transition are shown. Both of these spectra appear to have a very similar rotational structure. Unfortunately, the ( $3_0^1$ ) band is significantly weaker, prohibiting an extensive analysis as has been performed for its ( $0_0^0$ ) counterpart.

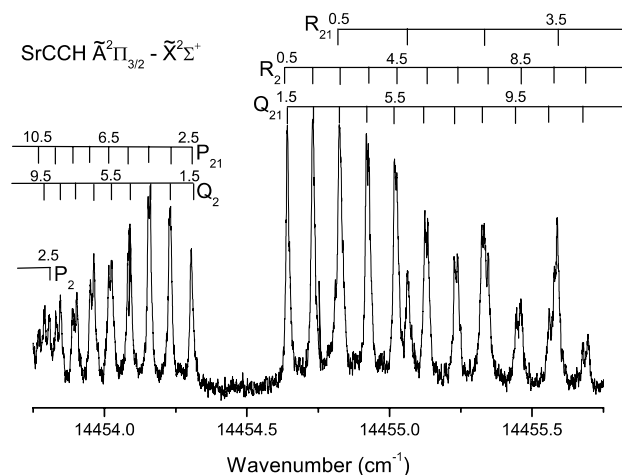


Fig. 4. A subsection of the high-resolution spectrum of the  $\tilde{A}^2\Pi_{3/2}-\tilde{X}^2\Sigma^+$  spin component of SrCCH. Assignments for each of the 6 possible branches are clearly labeled. At higher  $J$  values, a small splitting is observed between the  $R_2$  and  $Q_{21}$  branches and between the  $P_{21}$  and  $Q_2$  branches as a result of the spin rotation interaction in the ground state.

the  $\tilde{A}^2\Pi-\tilde{X}^2\Sigma^+$  transition of SrOH [30,31] as a guide. Initial  $J$  assignments were made using combination differences as described by Herzberg [32]. In Fig. 4, a subsection of the  ${}^2\Pi_{3/2}-{}^2\Sigma^+$  transition is shown with these  $J$  assignments. The data were analyzed using a Hund's case (a)  ${}^2\Pi$ —Hund's case (b)  ${}^2\Sigma^+$  rotational Hamiltonian in a nonlinear least squares fitting program. The usual  $\hat{N}^2$  Hamiltonian of Brown [33] was used. For the ( $0_0^0$ ) band of the  $\tilde{A}-\tilde{X}$  transition, a total of 118 lines listed in Table 1 were included in the fit, as well as the microwave data [11] previously measured for SrCCH. Rotational and fine structure parameters determined for both the  $\tilde{X}(0_0)$  and  $\tilde{A}(0_0)$  states are listed in Table 2. Because of the low  $J$  values measured in this study, centrifugal distortion terms, such as  $D$  and  $A_D$ , were not well determined for the  $\tilde{A}$  state.

For the ( $3_0^1$ ) band only a portion of the  ${}^2\Pi_{1/2}-{}^2\Sigma^+$  spin component was analyzable. A total of 23 lines from the  $P_1$ ,  $Q_{12}$ ,  $Q_1$ , and  $R_{12}$  branches were fit separately holding the  $\tilde{X}^2\Sigma^+(0_0)$  constants fixed to the values determined in the ( $0_0^0$ ) analysis. Additionally, the spin-orbit constant of the ( $3_1^1$ ) state was fixed to the ( $0_0^0$ ) value. As a result, only  $T$ ,  $B$ , and  $p$  (Table 2) values were determined for the ( $3_1^1$ ) vibrational level of the  $\tilde{A}$  state.

#### 4. Discussion

As a result of the rotational analysis of the  $\tilde{A}^2\Pi-\tilde{X}^2\Sigma^+$  transition of SrCCH a molecular structure can be calculated for the  $\tilde{A}$  state. Unfortunately, data for other isotopologues were not obtained, therefore some bond lengths must be assumed. Following the structure calculation for the  $\tilde{X}^2\Sigma^+$  state of SrCCH, the

Table 1  
Measured line positions (in  $\text{cm}^{-1}$ ) for the  $\tilde{A}^2\Pi-\tilde{X}^2\Sigma^+(0_0^0)$  transition

$^2\Pi_{1/2}-^2\Sigma^+$											
$J''$	$P_1(J)$	OMC	$R_1(J)$	OMC	$Q_1(J)$	OMC	$P_2(J)$	OMC	$R_2(J)$	OMC	$Q_2(J)$
0.5			14182.8560	-0.0239	14182.4924	0.0048					
1.5	14182.4184	0.0069	14183.1856	0.0026	14182.5379	0.0086	14181.9888	-0.0011	14182.5371	0.0053	14182.4184
2.5	14182.3794	0.0015	14183.4958	0.0064	14182.5788	0.0048	14181.6976	-0.0021	14182.5788	0.0005	14182.3794
3.5	14182.3503	0.0027	14183.7943	-0.0045	14182.6255	0.0036	14181.4187	0.0060	14182.6255	-0.0023	14182.3503
4.5	14182.3212	0.0008	14184.1136	0.0024	14182.6815	0.0088	14181.1348	0.0061	14182.6719	-0.0084	14182.3212
5.5	14182.3006	0.0043	14184.4318	0.0053	14182.7253	-0.0011			14182.7332	-0.0025	14182.3006
6.5	14182.2813	0.0061	14184.7407	-0.0038	14182.7804	-0.0023			14182.7893	-0.0044	14182.2813
7.5	14182.2519	-0.0051	14185.0676	0.0026	14182.8378	-0.0036			14182.8540	-0.0002	14182.2519
8.5	14182.2319	-0.0096	14185.3848	-0.0031	14182.9027	0.0002			14182.9147	-0.0022	14182.2319
9.5			14185.7164	0.0036	14182.9634	-0.0022			14182.9804	-0.0013	14182.2518
10.5			14186.0467	0.0071	14183.0261	-0.0043			14183.0468	-0.0014	14182.2518
11.5									14183.1138	-0.0024	
									14183.1945	0.0092	
$^2\Pi_{3/2}-^2\Sigma^+$											
$J''$	$P_2(J)$	OMC	$R_2(J)$	OMC	$Q_2(J)$	OMC	$P_{21}(J)$	OMC	$R_{21}(J)$	OMC	$Q_{21}(J)$
1.5			14454.6422	0.0005	14454.3053	-0.0037					
2.5	14453.8027	-0.0070	14454.7322	-0.0016	14454.2319	-0.0023	14454.3053	0.0005	14454.8100	0.0033	14454.6422
3.5	14453.5684	0.0002	14454.8239	-0.0050	14454.1605	-0.0019	14454.2319	0.0036	14455.0631	-0.0007	14454.7322
4.5	14453.3309	0.0011	14454.9257	-0.0014	14454.0903	-0.0032	14454.1540	-0.0008	14455.3317	0.0080	14454.8240
5.5	14453.0901	-0.0044	14455.0255	-0.0027	14454.0264	-0.0009	14454.0825	-0.0016	14455.5885	0.0019	14454.9187
6.5	14452.8602	-0.0019	14455.1339	0.0018	14453.9645	0.0008	14454.0165	0.0002	14455.8527	0.0005	14455.0171
7.5	14452.6304	-0.0022	14455.2376	-0.0011	14453.9037	0.0011	14453.9514	0.0004	14456.1212	0.0007	14455.1239
8.5	14452.4016	-0.0041	14455.3474	-0.0005	14453.8453	0.0015	14453.8891	0.0009	14456.3951	0.0039	14455.2263
9.5	14452.1798	-0.0016	14455.4610	0.0016	14453.7913	0.0042	14453.8290	0.0013	14456.6709	0.0068	14455.3237
10.5			14455.5781	0.0050	14453.7309	-0.0013	14453.7696	0.0003	14456.9464	0.0073	14455.4445
11.5			14455.6949	0.0061	14453.6774	-0.0015	14453.7030	-0.0097	14456.9464	0.0073	14455.4445
12.5			14455.7983	-0.0079	14453.6274	0.0006	14453.6615	0.0039	14456.9464	0.0073	14455.4445
13.5			14455.9227	-0.0023			14453.6053	0.0014	14456.9464	0.0073	14455.4445
14.5							14453.5449	-0.0063	14456.9464	0.0073	14455.4445
15.5							14453.4970	-0.0022	14456.9464	0.0073	14455.4445

Table 2  
Molecular parameters (in  $\text{cm}^{-1}$ ) determined for SrCCH

Parameter	$\tilde{X}^2\Sigma^+0_0$	$\tilde{A}^2\Pi 0^0$	$\tilde{A}^2\Pi 3^1$
$T$	0.0	14318.45764(78)	14663.4912(15)
$B$	0.08337782(16) <sup>a</sup>	0.084975(25)	0.086362(61)
$D \times 10^7$	0.26805(38)	10.5(1.4)	
$H \times 10^{14}$	6.48(29)		
$\gamma \times 10^3$	1.69664(94)		
$A$		272.1886(13)	272.1886
$A_D \times 10^4$		-1.13(20)	
$p$		-0.1101(34)	-0.05623(97)
$q \times 10^3$		9.3(1.7)	

<sup>a</sup> Values in parenthesis are  $1\sigma$  standard deviations, in units of the last significant digits.

C–H bond length was fixed to 1.056 Å and the C–C bond length at 1.204 Å [34]. Using the rotational constant obtained for the  $\tilde{A}$  state, the Sr–C bond length was calculated to be 2.43 Å. This value is slightly smaller than that observed for the ground state [11], 2.46 Å. MgCCH [26] and CaCCH [18] have also shown a similar decrease in the metal–carbon bond length from the ground state relative to first excited state. This effect has also been observed in other linear Sr containing molecules such as SrOH [30,31], and may likely be the result of the increase in the distance of the unpaired electron from the ligand in the  $\tilde{A}$  state as compared to the  $\tilde{X}$  state.

The vibrational frequency of the Sr–C stretch ( $\nu_3$ ) in the  $\tilde{A}$  state was also determined for SrCCH. This value, 345.0335  $\text{cm}^{-1}$ , is slightly smaller than the previously reported value of 354  $\text{cm}^{-1}$  [15], which was obtained using low-resolution techniques. Unfortunately, the vibrational frequency of the Sr–C stretch for the  $\tilde{X}$  state of SrCCH was not determined in the current work. However, a value of 343  $\text{cm}^{-1}$  was determined in the previous low-resolution work [15]. If the vibrational frequencies of the Sr–C stretch for the ground and first excited states are compared, a small increase in energy of only  $\sim 2 \text{ cm}^{-1}$  occurs. This suggests that the Sr–C bond strength is similar in both states. This change is much smaller than the  $\sim 55 \text{ cm}^{-1}$  increase recently observed for MgCCH [26].

Additionally, in this analysis the  $\Lambda$ -doubling parameter  $p$  of the  $\tilde{A}^2\Pi$  state of SrCCH was determined for the first time. As a result this constant can be compared to

those of the other alkaline-earth monoacetylides, MgCCH, and CaCCH. This comparison is useful for examining the validity of the pure precession relationships. Table 3 lists the  $\Lambda$ -doubling constants of the  $\tilde{A}$  state for the alkaline-earth monoacetylides. According to the pure precession relationships the  $p$  constant should be proportional to  $A_{\text{So}}/\Delta E(\tilde{A} - \tilde{B})$  and hence should become increasingly negative as long as the  $\tilde{B}$  state is the main perturber and is higher in energy than the  $\tilde{A}$  state. As mentioned in the recent work on MgCCH [26], small Mg containing molecules often do not follow this trend due to an interaction between the  $\tilde{A}$  state and a repulsive  $^2\Pi_i$  state and/or a spin polarization of the outer most two electrons on the ligand. However, for CaCCH and SrCCH  $p$  is negative and larger in magnitude for SrCCH. This follows the expected trend (i.e.,  $p(\text{SrCCH}) < p(\text{CaCCH})$ ) as the  $\tilde{B}^2\Sigma^+$  is expected to be closer in energy for SrCCH than for CaCCH. More work on the other alkaline-earth monoacetylides will be needed to see if this trend holds beyond SrCCH and CaCCH.

Assuming the pure precession relationships are valid for the alkaline-earth monoacetylides, the location of the  $\tilde{B}^2\Sigma^+$  state can be estimated using the expression,

$$p = \frac{2A_{\text{So}}B\ell(\ell + 1)}{E(\tilde{A}^2\Pi) - E(\tilde{B}^2\Sigma^+)}. \quad (1)$$

Using a value of  $\ell = 1$  for a  $p$  orbital, the  $\tilde{B}^2\Sigma^+$  state should be located  $\sim 840 \text{ cm}^{-1}$  above the  $\tilde{A}$  state or at  $\sim 15160 \text{ cm}^{-1}$ . As mentioned before, low-resolution survey scans obtained up to 16000  $\text{cm}^{-1}$  resulted in no observation of this state. Interestingly, a similar search conducted for CaCCH also failed to yield any evidence of the  $\tilde{B}$  state [17], suggesting that this state may be predissociative. The validity of this assumption can be determined using an absorption experiment, such as cavity ringdown spectroscopy.

## 5. Conclusions

This work is the first high-resolution spectroscopic study of the  $\tilde{A}^2\Pi - \tilde{X}^2\Sigma^+$  transition of SrCCH. The rotational analysis has confirmed a linear structure for SrCCH in the  $\tilde{A}^2\Pi$  excited state. Rotational and fine

Table 3  
Lambda doubling parameters<sup>a</sup> for MCCH species

State	Parameter	MgCCH <sup>b</sup>	CaCCH <sup>c</sup>	SrCCH <sup>d</sup>
$\tilde{A}^2\Pi$	$p$	$4.22(22) \times 10^{-4}$	-0.03016(1)	-0.1101(34)
	$q$	$2.99(28) \times 10^{-5}$	$-6.947(55) \times 10^{-5}$	$9.3(1.7) \times 10^{-3}$

<sup>a</sup> In  $\text{cm}^{-1}$ ; values in parenthesis are  $1\sigma$  standard deviations, in units of the last significant digits.

<sup>b</sup> From Ref. [26].

<sup>c</sup> From Ref. [18].

<sup>d</sup> This work.

structure parameters for the  $\tilde{A}$  state were determined, including, a spin orbit constant of  $272.1886\text{ cm}^{-1}$ , a rotational constant of  $0.084975\text{ cm}^{-1}$  and a vibrational frequency for the Sr–C stretch of  $345.0335\text{ cm}^{-1}$ . Using the rotational constant of the  $\tilde{A}$  state the Sr–C bond length was determined to be  $2.43\text{ \AA}$ , which is  $\sim 0.03\text{ \AA}$  shorter than in the ground state.  $\Lambda$ -doubling parameters have also been determined for the  $\tilde{A}$  state. A comparison of the  $p$  constant to those of the other alkaline-earth acetylides suggests that SrCCH and CaCCH appear to follow the pure precession relationship unlike MgCCH. Finally a search for the  $\tilde{B}^2\Sigma^+ - \tilde{X}^2\Sigma^+$  transition was not successful, as with CaCCH, suggesting that the  $\tilde{B}$  state may be predissociative.

### Acknowledgments

Financial support for this work was provided by the Natural Sciences and Engineering Research Council (NSERC) of Canada. In addition, the authors would like to thank Dr. T. C. Steimle for the loan of the Wavemeter Jr.

### References

- [1] H.-P. Loock, A. Bérces, B. Simard, *J. Chem. Phys.* 107 (1997) 2720–2727.
- [2] D.J. Brugh, R.S. DaBell, M.D. Morse, *J. Chem. Phys.* 121 (2004) 12379–12385.
- [3] A.J. Apponi, M.A. Brewster, L.M. Ziurys, *Chem. Phys. Lett.* 298 (1998) 161–169.
- [4] D.B. Grotjahn, A.J. Apponi, M.A. Brewster, J. Xin, L.M. Ziurys, *Angew. Chem. Int. Ed.* 37 (1998) 2678–2681.
- [5] M.A. Brewster, A.J. Apponi, J. Xin, L.M. Ziurys, *Chem. Phys. Lett.* 310 (1999) 411–422.
- [6] J. Xin, L.M. Ziurys, *Astrophys. J.* 501 (1998) L151–L153.
- [7] G. Scalmani, J.L. Brédas, V. Barone, *J. Chem. Phys.* 112 (2000) 1178–1191.
- [8] M.A. Anderson, L.M. Ziurys, *Astrophys. J.* 439 (1995) L25–L28.
- [9] M.A. Anderson, L.M. Ziurys, *Astrophys. J.* 444 (1995) L57–L60.
- [10] M. Li, J. Coxon, *J. Mol. Spectrosc.* 184 (1997) 395–400.
- [11] B.P. Nuccio, A.J. Apponi, L.M. Ziurys, *Chem. Phys. Lett.* 247 (1995) 283–288.
- [12] D.E. Woon, *Astrophys. J.* 456 (1996) 602–610.
- [13] D.E. Woon, *Chem. Phys. Lett.* 274 (1997) 299–305.
- [14] W.-T. Chan, I.P. Hamilton, *Chem. Phys. Lett.* 297 (1998) 217–224.
- [15] A.M.R.P. Bopegedra, C.R. Brazier, P.F. Bernath, *Chem. Phys. Lett.* 136 (1987) 97–100.
- [16] C.J. Whitham, B. Soep, J.-P. Visticot, A. Keller, *J. Chem. Phys.* 93 (1990) 991–1000.
- [17] A.M.R.P. Bopegedra, C.R. Brazier, P.F. Bernath, *J. Mol. Spectrosc.* 129 (1988) 268–275.
- [18] M. Li, J. Coxon, *J. Mol. Spectrosc.* 176 (1996) 206–210.
- [19] M. Li, J. Coxon, *J. Mol. Spectrosc.* 180 (1996) 287–297.
- [20] M. Li, J. Coxon, *J. Mol. Spectrosc.* 183 (1997) 250–262.
- [21] M. Li, J. Coxon, *J. Mol. Spectrosc.* 196 (1999) 14–19.
- [22] A.J. Marr, J. Perry, T.C. Steimle, *J. Chem. Phys.* 103 (1995) 3861–3863.
- [23] M. Elhanine, R. Lawruszczuk, B. Soep, *Chem. Phys. Lett.* 288 (1998) 785–792.
- [24] G.K. Corlett, M.S. Beardah, A.M. Ellis, *J. Mol. Spectrosc.* 185 (1997) 202–203.
- [25] G.K. Corlett, A.M. Little, A.M. Ellis, *Chem. Phys. Lett.* 249 (1996) 53–58.
- [26] D.W. Tokaryk, A.G. Adam, W.S. Hopkins, *J. Mol. Spectrosc.* 230 (2005) 54–61.
- [27] G.M. Greetham, A.M. Ellis, *J. Mol. Spectrosc.* 206 (2001) 198–199.
- [28] C. Zhao, P.G. Hajigeorgiou, P.F. Bernath, J.W. Hepburn, *J. Mol. Spectrosc.* 176 (1996) 268–273.
- [29] S. Gerstekorn, P. Luc, *Atlas du Spectre d’Absorption de la Molecule d’Iode Laboratoire Aimé-Cotton, CNRS II*, 91405, Orsay, France, 1978.
- [30] C.R. Brazier, P.F. Bernath, *J. Mol. Spectrosc.* 114 (1985) 163–173.
- [31] P.I. Presunka, J.A. Coxon, *Chem. Phys. Lett.* 190 (1995) 97–111.
- [32] G. Herzberg, *Molecular Spectra and Molecular Structure*, vol. I—Spectra of Diatomic Molecules, Krieger Publishing Company, Malabar FL, 1989.
- [33] J.M. Brown, E.A. Colbourn, J.K.G. Watson, F.D. Wayne, *J. Mol. Spectrosc.* 74 (1979) 294–318.
- [34] *Handbook of Chemistry and Physics*, 63rd ed., CRC Press, Boca Raton, FL, 1982.